Photonic Patterns

Deutsche Ausgabe: DOI: 10.1002/ange.201410411
Internationale Ausgabe: DOI: 10.1002/anie.201410411

Photonic Patterns Printed in Chiral Nematic Mesoporous Resins**

*Mostofa K. Khan, Anas Bsoul, Konrad Walus, Wadood Y. Hamad, and Mark J. MacLachlan**

Abstract: *Chiral nematic mesoporous phenol-formaldehyde resins, which were prepared using cellulose nanocrystals as a template, can be used as a substrate to produce latent photonic images. These resins undergo swelling, which changes their reflected color. By writing on the films with chemical inks, the density of methylol groups in the resin changes, subsequently affecting their degree of swelling and, consequently, their color. Writing on the films gives latent images that are revealed only upon swelling of the films. Using inkjet printing, it is possible to make higher resolution photonic patterns both as text and images that can be visualized by swelling and erased by drying. This novel approach to printing photonic patterns in resin films may be applied to anti-counterfeit tags, signage, and decorative applications.*

Encrypting data[1–3] and designing sensors[4] that can discriminate various stimuli rely on the ability to encode complex chemical information. For example, fluidic and diagnostic devices have been made by spatial encoding of hydrophilicity in three-dimensional porous networks.[5] Color-changing materials have garnered tremendous interest for their potential applications in encryption,[6] sensing,[7] optoelectronics,[8] and displays.[9] To that end, much research effort has been invested to construct photonic structures in synthetic materials and integrating these into devices.[10] Bragg stacks, 3D opals, and block copolymer gels are examples of structures that are being explored for their photonic properties.[11] The use of liquid-crystal templates to embed structures has emerged as a promising bottom-up approach to synthesize photonic materials.

Patterned photonic crystals have potential applications in optical, display, and microfluidic devices.[12–14] Photonic crystals are generally patterned by lithographic techniques or self-assembly of colloidal particles. Traditional lithographic patterning is complex, time consuming, and costly for large-scale generation and hence prohibitive for many applications. Because of that, self-assembly of colloidal particles has been widely explored and used to prepare patterned photonic structures through magnetic alignment,[15] extrusion and compression molding,[16] capillary force-induced infiltration,[17] or triphase microfluidic-directed assembly[18] followed by fixation in a polymer host. Patterning by the self-assembly of colloidal particles is limited by characteristics of the template and a multi-step fabrication procedure. Color tuning of the patterns was attained primarily by varying the size of the colloidal particles and secondarily tuning the lattice constant by strain (in cases of elastomeric polymer matrix)[16,19] or by swelling/deswelling of the polymer matrix in appropriate solvents.[20] Recently, macroscale patterned photonic crystals were fabricated by ink-jet printing using colloidal particle dispersions as ink.[21] Although simple, this technique relies on localized self-assembly of colloids that suffers from inevitable crystal defects caused by disturbances from ambient environment during the self-assembly process and thus inhomogeneity in color. Moreover, the inconvenience of substrate surface pretreatment to make it compatible with the ink and in many cases the lack of required flexibility of the substrate limits its widespread application.

Cellulose nanocrystals (CNCs)[22–25] can be used to template mesoporous chiral nematic materials with photonic properties.[26–29] In these structures, the pores are aligned in layers, but their orientation within the layers rotates through the stack. This chiral nematic organization leads to the selective reflection of circularly polarized light with a wavelength (i.e., color) that depends both on the pitch of the helicoidal structure and the refractive index. This concept was extended to phenol-formaldehyde (PF) resins to give flexible, mesoporous photonic resins.[30,31] Photonic properties arising from the chiral nematic structure of CNCs have been exploited to produce predefined watermark-like patterns in solid iridescent films of CNCs by differential heating of a CNC dispersion during film casting, or by changing the hydrophobicity of the substrate.[32] We recently used CNC templates to construct patterns in responsive hydrogels by regioselective crosslinking through photomasking.[33] Also, permanent photonic patterns were imprinted in amino-formaldehyde/CNC composite films by applying external pressure to cause an irreversible change in helical pitch of the chiral nematic structure, creating color contrast.[34]

[*] Dr. M. K. Khan, Prof. M. J. MacLachlan
Department of Chemistry, University of British Columbia
2036 Main Mall, Vancouver, BC, V6T 1Z1 (Canada)
E-mail: mmaclach@chem.ubc.ca
Homepage: http://www.chem.ubc.ca/mark-maclachlan
A. Bsoul
Department of Electrical and Computer Engineering
University of British Columbia
2332 Main Mall, Vancouver, BC, V6T 1Z4 (Canada)
and
Department of Computer Engineering
Jordan University of Science and Technology
Irbid (Jordan)
Prof. K. Walus
Department of Electrical and Computer Engineering
University of British Columbia
2332 Main Mall, Vancouver, BC, V6T 1Z4 (Canada)
Dr. W. Y. Hamad
FPInnovations
2665 East Mall, Vancouver, BC, V6T 1Z4 (Canada)

[**] We thank NSERC for funding and CelluForce Inc. for cellulose nanocrystals.

Supporting information for this article is available on the WWW under http://dx.doi.org/10.1002/anie.201410411.

Herein we present a novel way to pattern photonic PF resins by ink-jet printing. The patterns can be reversibly revealed and concealed upon swelling and drying, respectively.

The chiral nematic mesoporous polymers were synthesized according to the procedure reported before (Scheme 1).[30] In a representative procedure, an aqueous

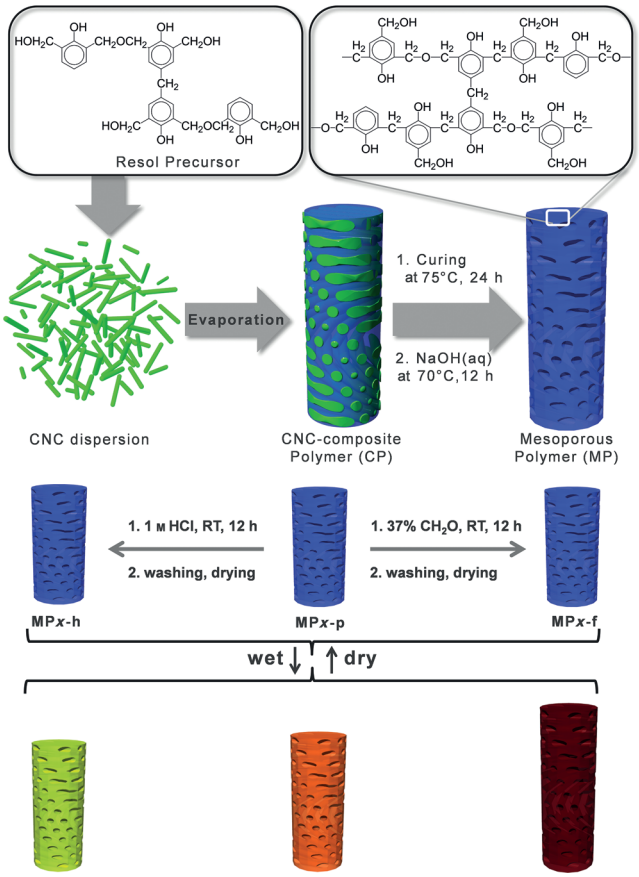

Scheme 1. Synthesis of chiral nematic mesoporous PF resin films. An aqueous mixture of CNCs and PF polymer precursor was dried to give chiral nematic composite films (CP). Alkaline treatment of the composites removes the CNC template, giving highly iridescent, mesoporous photonic resins (MP). Treatment of as-synthesized mesoporous-resin films (MPx-p; $x=1$ or 2) with HCl and formaldehyde results in MPx-h and MPx-f films, respectively, which show different reflected color upon swelling in polar solvents.

CNC dispersion was mixed with a solution of the PF precursor in a water/ethanol mixture, then dried to give iridescent chiral nematic composite films. Subsequent curing of the films at 75 °C resulted in slight shrinkage of the film and a blue shift in the reflection color by about 15–20 nm (composite polymer (CP) samples). Pliable, mesoporous-resin films were obtained by treating the composite films with $NaOH_{aq}$ at 70 °C to remove CNCs, then drying the films from supercritical CO_2 (mesoporous polymer (MP) samples). The films appear iridescent and the coloration of the films arises from the chiral nematic organization of CNCs embedded in the materials.

The wavelength of the reflected light (λ_{max}) viewed perpendicular to a film with chiral nematic order is proportional to both the average refractive index (n_{avg}) and the helical pitch.[35] The color of the composite films can be red-shifted by increasing the ratio of PF precursor to CNCs or, conversely, blue-shifted by addition of salts.[30] By employing these strategies, we synthesized two samples with different colors (Figure S1 a). The change in color arises from the change in the helical pitch of the chiral nematic structure. The reflected wavelengths of the composite samples at normal incidence were at 500 nm for sample **CP1** and 440 nm for sample **CP2**. Polarized optical microscopy (POM) images (Figure S1 b,c) showed strong birefringence and fingerprint textures that are characteristic of chiral nematic organization. The films selectively reflect left-handed circularly polarized light, as confirmed by the intense positive signals observed in the circular dichroism (CD) spectra (solid lines, Figure 1 a).

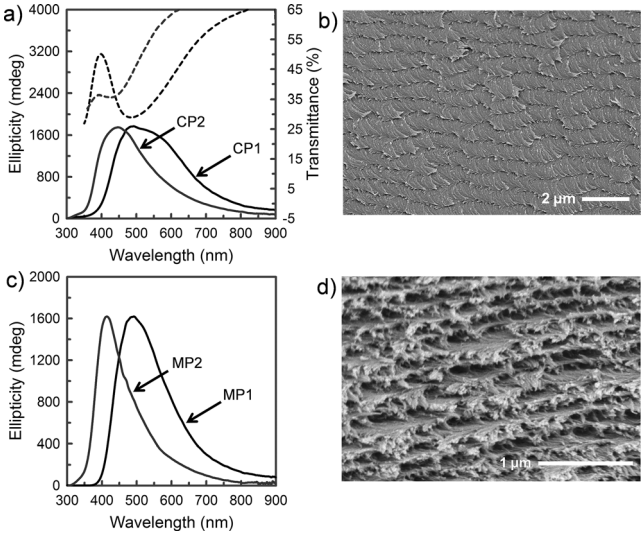

Figure 1. a) UV-Vis (dashed lines) and CD (solid lines) spectra of **CP1** and **CP2** composite films; b) SEM image at fracture section of **CP1** showing twisted layered structure; c) CD spectra of **MP1** and **MP2** mesoporous-resin films; and d) SEM image of **MP1** resin film showing twisted layered structures retained after removal of CNCs.

These CD signals correspond to the reflection wavelengths measured by UV-Vis spectroscopy (dashed lines, Figure 1 a). Scanning electron microscopy (SEM) images (Figure 1 b, Figure S2) also show a layered, twisted structure for the polymer composites that is consistent with a left-handed chiral nematic organization. Taken together, these investigations confirm that the observed reflections arise from the chiral nematic order of the polymer composites.

Thermal curing below 100 °C enhances polymerization of the PF resin precursor to give highly iridescent but brittle composite films. Treatment with aqueous NaOH removes 80–90 % of the CNC template from the composite films, resulting in mesoporous films with significantly improved mechanical properties.[30] Retention of the chiral nematic order in the samples after CNC removal was confirmed by POM, SEM, and CD measurements. POM images (Figure S3 a) of sample **MP1** show strong birefringence that is indicative of a chiral

nematic material. Although the resin itself is amorphous, the anisotropic structure of the resin with a chiral nematic arrangement of pores gives rise to the optical anisotropy (i.e., form birefringence). CD spectra of mesoporous-resin films (Figure 1c) show intense signals with positive ellipticity. Samples **MP1** and **MP2** were obtained as flexible, iridescent films with blue-shifted reflection peak wavelengths (485 nm and 415 nm for **MP1** and **MP2**, respectively). The twisted layered structure is evident from SEM images (Figure 1d, Figure S3b–d) further confirming the retention of the chiral nematic structure after removal of the CNCs.

The mesoporous PF films are hydrophilic, an indication that they are mainly uncrosslinked with a high density of methylol groups; this is expected as the maximum curing temperature that was used was 75 °C (Scheme 1).[36] The mesoporous-resin films show more red-shifted color when soaked in water than in ethanol, despite the similar refractive indices of both solvents. This observation confirms that although the infiltration of pores with solvents results in a net increase in the average refractive index of the materials, the red-shift in color is mainly caused by the lengthening of the helical pitch upon swelling.

Methylol groups in the resin films can undergo additional reactions, and crosslinking by acidification, forming methylene ether bonds.[37] On the other hand, the concentration of methylol groups in the pores may be increased by reacting surface phenol rings with more formaldehyde. These two methods, acidification and addition of formaldehyde, offer routes to decrease and increase, respectively, the concentration of methylol groups on the surface of the material. Figure S4 shows the IR spectra of **MP1** resin film treated with hydrochloric acid (blue) and formaldehyde (red), and the as-synthesized film (green) (henceforth referred to as **MP1-h**, **MP1-f** and **MP1-p**, respectively; Scheme 1). Spectra of all three samples show an intense broad band at around 3340 cm^{-1} from the O–H stretch of hydrogen-bonded phenolic groups and a peak at around 2890 cm^{-1} from the C–H stretch of methylene (CH_2) groups. In addition, two relatively strong bands at 1639 and 1609 cm^{-1} are attributed to an aromatic ring stretch arising from mixtures of 1,2,4- and 1,2,6-trisubstituted as well as phenyl–alkyl ether-type substituted aromatic rings. For **MP1-p**, the band at 1609 cm^{-1} has relatively higher intensity than that at 1637 cm^{-1}, whereas in both **MP1-h** and **MP1-f**, there is an intensity reversal in those two peaks. The variation in relative intensities of these peaks clearly indicates different extent of (tri- vs. tetra-) substitutions of the aromatic rings caused by crosslinking through acidification with HCl, and formation of methylol groups by addition of formaldehyde.[38] Thermogravimetric analysis of the samples under air showed distinct degradation profiles (Figure S5a). All three samples show a weight loss of around 5% below 160 °C, attributed to the loss of adsorbed moisture and other volatile organics. **MP1-p** is stable to around 300 °C and degradation occurs in three distinct stages between 300–515 °C. On the other hand, **MP1-f** starts degradation at a lower temperature (270 °C), causing release of formaldehyde and other degradation by-products through condensation of methylol groups. Degradation of **MP1-f** is completed at the same temperature as that for **MP1-p** (515 °C). In contrast, **MP1-h** shows a significant weight loss of approximately 20% at a much lower temperature compared to the other two samples. This observation can be attributed to the release of adsorbed water and HCl that remained in the materials. However, after the initial weight loss, **MP1-h** showed improved thermal stability (by about 50 °C) compared to both **MP1-p** and **MP1-f**, indicating enhanced crosslinking caused by acidification. This was further confirmed by differential scanning calorimetry of the corresponding samples. All three samples showed an exothermic peak at temperatures (centered at around 495 °C for both **MP1-p** and **MP1-f** and at 555 °C for **MP1-h**) corresponding to their final stage of degradation (Figure S5b–d). In addition, sample **MP1-p** shows an endothermic peak at 356 °C that was attributed to the condensation of methylol groups with phenol or other methylol groups forming methylene or dibenzyl ether bridges, respectively, and thereby releasing formaldehyde.[39] A similar but more intense endothermic peak is observed at 280 °C for **MP1-f**, indicating the presence of more methylol groups obtained by the post-synthetic addition of formaldehyde. However, the acid-treated sample **MP1-h** did not show any endothermic peak in that temperature region (Figure S5b), confirming that most of the methylol groups are condensed by acidification with HCl, leading to enhanced crosslinking.

Variation in the number of polar methylol groups is also reflected in their surface properties. Among these samples, **MP1-p** showed a static contact angle of $61 \pm 1.3°$, while **MP1-h** showed highest contact angle of $69 \pm 1.1°$ and the **MP1-f** showed the lowest contact angle of $54 \pm 1.3°$ (Figure 2a). Thus, with acidification, the film becomes less hydrophilic, consistent with a lower concentration of methylol groups on the surface. In contrast, treatment of the film with formaldehyde renders it more hydrophilic. This variation in contact angle implies that there should be a difference in the extent of swelling of these materials in polar solvents. Figure 2b shows the photographs of **MP1-p** (middle), **MP1-h** (left) and **MP1-f** (right) films. The corresponding CD spectra are shown in Figure 2c. Both **MP1-p** and **MP1-h** showed reflection peaks at 495 nm, while **MP1-f** showed a slightly red-shifted peak at 515 nm in the dry state. However, all three samples showed substantially red-shifted reflection peaks when they are soaked in water. This red shift in reflection color is clearly visible and is attributed primarily to the lengthening of the helical pitch by swelling. The extent of swelling can be controlled by changing the solvent polarity, as shown here with binary mixtures of ethanol and water (Figure 2b middle). Upon complete swelling in water, the pristine **MP1-p** sample showed a reflection peak at 730 nm (a shift of 235 nm from its dry state). For comparison, upon swelling in water, **MP1-h** showed a reflection red-shifted by only 110 nm (reflection peak at 605 nm) and **MP1-f** showed a large red-shift of 320 nm (reflection peak at 835 nm). The difference in the reflected color from sample to sample changes relatively with the polarity of the solvent, as shown in the photographs in Figure 2b. This provides an easy means to modulate the extent of swelling and hence the reflected color of the mesoporous photonic PF resins.

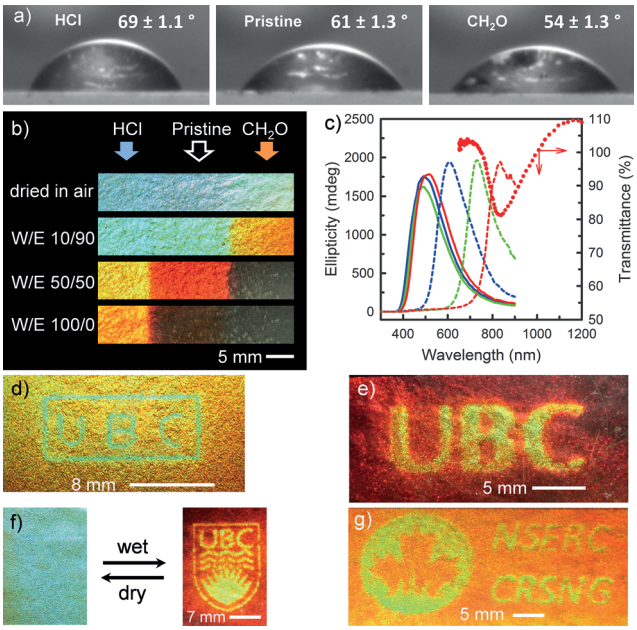

Figure 2. a) Images from static contact angle measurements of **MP1** resin films treated with HCl (left), pristine (middle), and treated with CH_2O (right); b) photographs of a strip of **MP1** resin films showing the changes in color in water/ethanol binary solvent mixtures of different proportions. The left and right ends of the strip were treated with HCl (**MP1-h**) and CH_2O (**MP1-f**), respectively, while the middle part remained untreated (**MP1-p**); c) CD spectra of **MP1-p** (green), **MP1-h** (blue), and **MP1-f** (red) resin films in dry state (solid lines) and after swelling in water (dashed lines). As the CD spectrometer that was used cannot measure beyond 900 nm, the reflection peak of **MP1-f** in the swollen state was confirmed with complementary UV-Vis spectroscopy (red dotted line). Inkjet printing of photonic patterns on mesoporous-resin films: d) pattern printed as letters "UBC" on **MP2** resin films, e) "UBC" patterned as an image, f) and g) more complicated images patterned on **MP1** resin film. The pattern in (f) was revealed by swelling in water while the pattern in (g) was revealed in 20/80 (v/v) water/ethanol mixture. The appearance and disappearance of the patterns upon swelling and drying, respectively, are completely reversible.

In an attempt to print photonic patterns on the mesoporous-resin films, 2 μL drops of 1 M HCl_{aq} were deposited in an array of letters and dried under ambient conditions. After washing the film with distilled water to remove unreacted HCl followed by complete swelling in water, photonic patterns were observed (Figure S6a,b). It was also possible to write letters on the resin films with a home-made pen using HCl as ink (Figure S6c), but the pen tip tended to scratch the surface of the film.

Inspired by the success of these preliminary experiments, we investigated inkjet printing to pattern the resin films. We employed a custom-made inkjet printer to print patterns on the resin films using 1 M HCl_{aq} solution as "ink".[40] With inkjet printing, we were able to print characters "UBC" on **MP2** as text (Figure 2d) as well as an image on **MP1** (Figure 2e). This high-throughput, yet simple printing technique can be used to print even more complicated patterns on a resin film (Figure 2f and g), underscoring the general utility of this printing technique. The appearance and disappearance of the patterns upon swelling and drying are completely reversible for many cycles (Figure S7). The colors of the patterns or the matrix can be varied (compare Figure 2d and e) by tuning the helical pitch of the original resin films during their synthesis (by changing the ratio of CNC to resin precursor or by adding salts). Alternatively, the color can be tuned after the synthesis with solvents of different polarity (Figure 2b and g). This is a unique property of these materials, where the outward appearance of the resulting patterns can be easily tuned on demand.

In summary, we demonstrated a new way to pattern mesoporous phenol-formaldehyde resins. Upon swelling in polar solvents, the photonic resin shows red-shifted color, which can be manipulated by treating the film with either acid or formaldehyde. With acidification, the films show enhanced crosslinking, a lower density of surface methylol groups, and hence lower hydrophilicity. In contrast, films treated with formaldehyde show an increased density of methylol groups and thus increased hydrophilicity. These changes result in a difference in the extent of swelling of the films in polar solvents, which changes the pitch in the chiral nematic structure and, consequently, the reflected color. By applying acid or formaldehyde to regions of the films, it is possible to produce latent images that are presented only upon swelling of the film. Using inkjet printing, it was possible to print both text and images as higher-resolution photonic patterns that can be visualized by swelling and erased by drying. This is the first example of printing photonic patterns in PF resin films, and these materials may be used as anti-counterfeiting materials in security documents, in visual graphic signage and in decorative applications.

Keywords: cellulose nanocrystals · liquid-crystal template · mesoporous material · photonic pattern · resins

How to cite: *Angew. Chem. Int. Ed.* **2015**, *54*, 4304–4308
Angew. Chem. **2015**, *127*, 4378–4382

[1] S. W. Thomas, R. C. Chiechi, C. N. LaFratta, M. R. Webb, A. Lee, B. J. Wiley, M. R. Zakin, D. R. Walt, G. M. Whitesides, *Proc. Natl. Acad. Sci. USA* **2009**, *106*, 9147.
[2] D. Margulies, C. E. Felder, G. Melman, A. Shanzer, *J. Am. Chem. Soc.* **2007**, *129*, 347.
[3] C. T. Clelland, V. Risca, C. Bancroft, *Nature* **1999**, *399*, 533.
[4] K. I. MacConaghy, C. I. Geary, J. L. Kaar, M. P. Stoykovich, *J. Am. Chem. Soc.* **2014**, *136*, 6896.
[5] a) J.-T. Lee, M. C. George, J. S. Moore, P. V. Braun, *J. Am. Chem. Soc.* **2009**, *131*, 11294; b) A. W. Martinez, S. T. Phillips, G. M. Whitesides, *Proc. Natl. Acad. Sci. USA* **2008**, *105*, 19606.
[6] I. B. Burgess, L. Mishchenko, B. D. Hatton, M. Kolle, M. Lončar, J. Aizenberg, *J. Am. Chem. Soc.* **2011**, *133*, 12430.
[7] a) I. B. Burgess, M. Lončar, J. Aizenberg, *J. Mater. Chem. C* **2013**, *1*, 6075; b) L. D. Bonifacio, D. P. Puzzo, S. Breslav, B. M. Willey, A. McGeer, G. A. Ozin, *Adv. Mater.* **2010**, *22*, 1351.
[8] A. Arsenault, S. Fournier-Bidoz, B. Hatton, H. Míguez, N. Tétreault, E. Vekris, S. Wong, S. M. Yang, V. Kitaev, G. A. Ozin, *J. Mater. Chem.* **2004**, *14*, 781.
[9] Y. Zhao, Z. Xie, H. Gu, C. Zhu, Z. Gu, *Chem. Soc. Rev.* **2012**, *41*, 3297.
[10] a) Z. Wang, J. Zhang, J. Xie, Y. Yin, Z. Wang, H. Shen, Y. Li, J. Li, S. Liang, L. Cui, L. Zhang, H. Zhang, B. Yang, *ACS Appl. Mater. Interfaces* **2012**, *4*, 1397; b) G. von Freymann, V. Kitaev, B. V. Lotsch, G. A. Ozin, *Chem. Soc. Rev.* **2013**, *42*, 2528.

[11] a) L. D. Bonifacio, B. V. Lotsch, D. P. Puzzo, F. Scotognella, G. A. Ozin, *Adv. Mater.* **2009**, *21*, 1641; b) J. H. Moon, S. Yang, *Chem. Rev.* **2010**, *110*, 547; c) H. S. Lim, J.-H. Lee, J. J. Walish, E. L. Thomas, *ACS Nano* **2012**, *6*, 8933.
[12] T. Kaji, T. Yamada, S. Ito, H. Miyasaka, R. Ueda, S.-i. Inoue, A. Otomo, *J. Am. Chem. Soc.* **2013**, *135*, 106.
[13] P. Kang, S. O. Ogunbo, D. Erickson, *Langmuir* **2011**, *27*, 9676.
[14] Y. Zeng, M. He, D. J. Harrison, *Angew. Chem. Int. Ed.* **2008**, *47*, 6388; *Angew. Chem.* **2008**, *120*, 6488.
[15] a) L. He, M. Wang, J. Ge, Y. Yin, *Acc. Chem. Res.* **2012**, *45*, 1431; b) H. Hu, H. Zhong, C. Chen, Q. Chen, *J. Mater. Chem. C* **2014**, *2*, 3695.
[16] C. G. Schäfer, M. Gallei, J. T. Zahn, J. Engelhardt, G. P. Hellmann, M. Rehahn, *Chem. Mater.* **2013**, *25*, 2309.
[17] H. S. Lee, T. S. Shim, H. Hwang, S.-M. Yang, S.-H. Kim, *Chem. Mater.* **2013**, *25*, 2684.
[18] Z. Yu, C.-F. Wang, L. Ling, L. Chen, S. Chen, *Angew. Chem. Int. Ed.* **2012**, *51*, 2375; *Angew. Chem.* **2012**, *124*, 2425.
[19] T. Ito, C. Katsura, H. Sugimoto, E. Nakanishi, K. Inomata, *Langmuir* **2013**, *29*, 13951.
[20] H. Fudouzi, Y. Xia, *Langmuir* **2003**, *19*, 9653.
[21] J. Wang, L. Wang, Y. Song, L. Jiang, *J. Mater. Chem. C* **2013**, *1*, 6048.
[22] Y. Habibi, L. A. Lucia, O. J. Rojas, *Chem. Rev.* **2010**, *110*, 3479.
[23] D. Klemm, F. Kramer, S. Moritz, T. Lindström, M. Ankerfors, D. Gray, A. Dorris, *Angew. Chem. Int. Ed.* **2011**, *50*, 5438; *Angew. Chem.* **2011**, *123*, 5550.
[24] W. Y. Hamad, T. Q. Hu, *Can. J. Chem. Eng.* **2010**, *88*, 392.
[25] B. L. Peng, N. Dhar, H. L. Liu, K. C. Tam, *Can. J. Chem. Eng.* **2011**, *89*, 1191.
[26] J. A. Kelly, M. Giese, K. E. Shopsowitz, W. Y. Hamad, M. J. MacLachlan, *Acc. Chem. Res.* **2014**, *47*, 1088.
[27] K. E. Shopsowitz, H. Qi, W. Y. Hamad, M. J. MacLachlan, *Nature* **2010**, *468*, 422.
[28] K. E. Shopsowitz, W. Y. Hamad, M. J. MacLachlan, *J. Am. Chem. Soc.* **2012**, *134*, 867.
[29] A. S. Terpstra, K. E. Shopsowitz, C. F. Gregory, A. P. Manning, C. A. Michal, W. Y. Hamad, J. Yang, M. J. MacLachlan, *Chem. Commun.* **2013**, *49*, 1645.
[30] M. K. Khan, M. Giese, M. Yu, J. A. Kelly, W. Y. Hamad, M. J. MacLachlan, *Angew. Chem. Int. Ed.* **2013**, *52*, 8921; *Angew. Chem.* **2013**, *125*, 9089.
[31] M. K. Khan, W. Y. Hamad, M. J. MacLachlan, *Adv. Mater.* **2014**, *26*, 2323.
[32] a) S. Beck, J. Bouchard, G. Chauve, R. Berry, *Cellulose* **2013**, *20*, 1401; b) T.-D. Nguyen, W. Y. Hamad, M. J. MacLachlan, *Chem. Commun.* **2013**, *49*, 11296.
[33] J. A. Kelly, A. M. Shukaliak, C. C. Y. Cheung, K. E. Shopsowitz, W. Y. Hamad, M. J. MacLachlan, *Angew. Chem. Int. Ed.* **2013**, *52*, 8912; *Angew. Chem.* **2013**, *125*, 9080.
[34] M. Giese, M. K. Khan, W. Y. Hamad, M. J. MacLachlan, *ACS Macro Lett.* **2013**, *2*, 818.
[35] a) J.-F. Revol, L. Godbout, D. G. Gray, *J. Pulp Pap. Sci.* **1998**, *24*, 146; b) H. De Vries, *Acta Crystallogr.* **1951**, *4*, 219.
[36] G. E. Maciel, I. S. Chuang, L. Gollob, *Macromolecules* **1984**, *17*, 1081.
[37] G. He, B. Riedl, A. Aït-Kadi, *J. Appl. Polym. Sci.* **2003**, *87*, 433.
[38] Y. J. Kim, M. I. Kim, C. H. Yun, J. Y. Chang, C. R. Park, M. Inagaki, *J. Colloid Interface Sci.* **2004**, *274*, 555.
[39] Y.-K. Lee, D.-J. Kim, H.-J. Kim, T.-S. Hwang, M. Rafailovich, J. Sokolov, *J. Appl. Polym. Sci.* **2003**, *89*, 2589.
[40] A. Bsoul, S. Beyer, A. Ahmadi, B. Stoeber, E. Cretu, K. Walus, *MicroTAS* **2013**, 636.

Received: November 6, 2014
Revised: December 24, 2014
Published online: February 12, 2015

